D4.2

Test-bed based assessment and proof of concept

Project number:	619086
Project acronym:	**MAMMOET**
Project title:	Massive MIMO for Efficient Transmission
Project Start Date:	1 January, 2014
Duration:	36 months
Programme:	FP7/2007-2013

Deliverable Type:	Report
Reference Number:	ICT-619086-D4.2
Workpackage:	WP 4
Due Date:	30 September, 2016
Actual Submission Date:	4 October, 2016

Responsible Organisation:	ULUND
Editor:	Ove Edfors
Dissemination Level:	PU
Revision:	0.1

Abstract:	This deliverable details the testbed based assessment and proof-of-concept studies performed in the MAMMOET project. The real-time testbed architecture and implementation is described, together with system parameters. Both indoor and outdoor tests are described, where the behaviour of MaMi communication is studied. Tests are performed both in stationary (indoor/outdoor) and mobile (outdoor) environments.
Keywords:	testbed, proof-of-concept, indoor, outdoor, mobility

This project has received funding from the European Union's Seventh Framework Programme for research, technological development and demonstration under grant agreement no. 619086.

Editor

Ove Edfors(ULUND)

Contributors (ordered according to beneficiary numbers)

Ove Edfors, Fredrik Tufvesson, Liang Liu, Steffen Malkowsky, Joao Vieira (ULUND)
Liesbet Van der Perre (KUL)
Emil Björnson, Erik G. Larsson (LIU)

Executive Summary

This deliverable focuses on the experiments carried out in the LuMaMi massive MIMO testbed, developed at Lund University (ULUND) during the MAMMOET project. Both the testbed itself and some of the important proofs-of-concept tests performed are being detailed. In particular, design and architecture of the testbed, including important physical layer parameters, are described. The presented proofs-of-concept show that massive MIMO (MaMi) works well in different environments, both indoor and outdoor, and can handle highly mobile scenarios – in these tests up to 50 km/h. The general conclusion is that real-time LTE-like MaMi can be implemented with standard hardware (software-defined radios) and performs as expected from communication theory. The tests show that more elaborate linear precoders/detectors are often needed in real scenarios, since the basic maximum-ratio transmission/combining does not provide enough isolation between users. Using zero-forcing significantly improves the signal quality and spatial multiplexing works well.

Contents

List of Figures

List of Tables

Chapter 1

Introduction

When introducing a new technology, like massive MIMO (MaMi), there is always a number of critical points to address from a practical implementation point of view. Especially in the case of MaMi, there was initial skepticism regarding the extraordinary properties promised by theoretical investigations. Theory predicts orders-of-magnitude improvements of both spectral and energy efficiencies, compared to traditional wireless systems. Would these hold up when operating MaMi implemented with conventional hardware in real propagation environments?

Throughout the MAMMOET project we have been able to verify most of the MaMi claims, through simulations, channel measurements, and implementation of a real-time MaMi testbed. This deliverable deals with the proofs-of-concept performed on that testbed.

The MaMi testbed developed during the MAMMOET project consists of a 100-antenna base station and 12 single-antenna terminals, capable of real-time communication based on an LTE-like physical layer. Through this we have provided the means to perform several important proofs-of-concept. In some of the experiments we have teamed up with University of Bristol to exploit the synergy effects of having similar testbeds, built using the same hardware and software. University of Bristol is not a partner in MAMMOET, but teaming up with them (at no extra cost for MAMMOET) has allowed us to take the proof-of-concept studied further than initially planned and budgeted for in the MAMMOET project.

In this deliverable, we describe the testbed hardware and software, system parameters, and some of the experiments performed to show that MaMi works well in different environments and can handle user mobility.

Chapter 2

Testbed overview

Before we describe the proof-of-concept tests performed in the context of MAMMOET, we describe the architecture/design of the testbed and its physical layer parametrization, including modulation schemes, frame structure, channel estimation, payload data transmission and the linear precoding/detection schemes used. We would like to point out that although system parameters adopted in these tests resemble those of LTE systems, the system can also operate with other settings.

2.1 Architecture and design

The Lund University MaMi (LuMaMi) testbed is shown in Figure 2.1. It constitutes a fully reconfigurable real-time testing platform for MaMi. The system consist of 50 Software-defined radios (SDRs), four centralized co-processor, four PXIe chassis, 8 Octoclock and a standard windows-based host computer. The SDRs provide two RF-chains each and are, like the co-processor, fully reconfigurable by utilizing an internal Kintex-7 FPGA. The chassis employ PXIe interfaces to interconnect all the SDRs and co-processors in the system through PCIe switches.

As shown in Figure 2.1 left, synchronization is performed through connecting all SDRs to a centrally localized timing module utilizing the 8 octoclocks (OC) for the distribution network. Via this network, a 10 MHz reference clock and a pulse-per-second (PPS) signal are shared to time and frequency align the whole system.

Wireless signaling is performed through a 160 element dual polarized antenna array as given in Figure 2.1 right. As the 50 utilized SDRs provide 100 RF chains, 100 elements are connected at a time, the T-shape form allows to experiment with different antenna arrangement patterns, e.g. 4×25 or 10×10, with the first option being the default configuration.

Figure 2.2 details the system partitioning and processing distribution on the devices. The 50 SDRs are divided in groups of up to eight. For the LuMaMi testbed using 50 SDRs, the system is divided into seven groups of eight SDRs plus a single group with two SDRs. On the SDRs, per-antenna processing is performed, i.e. OFDM modulation and demodulation including cyclic prefix addition/removal. Two high-speed routers are used within each group to aggregate/disaggregate the data from the up to 16 antennas within the group (Antenna Combiner/BW splitter on the UL and Antenna Splitter/BW combiner on the DL) to cope with the limited number of inter-FPGA links. Consequently, the overall bandwidth is split into 4 subbands each representing one quarter of the 20 MHz bandwidth.

The centralized MIMO processing is performed on the four co-processors, each working on all antennas but the aforementioned limited set of subcarriers corresponding to one quarter of the

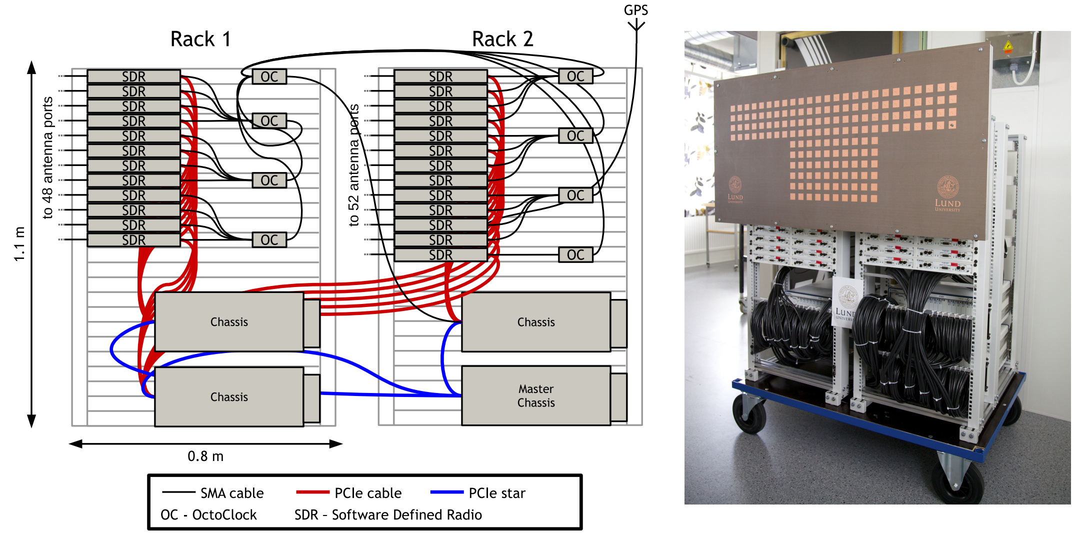

Figure 2.1: Left: Side view of the mechanical assembly of the BS. The two racks sit side by side (not as shown) with the SDRs facing the same direction (towards the antenna array). Two columns of USRP SDRs are mounted in each rack, totaling 50 of them. Right: The assembled LuMaMi testbed at Lund University, Sweden.

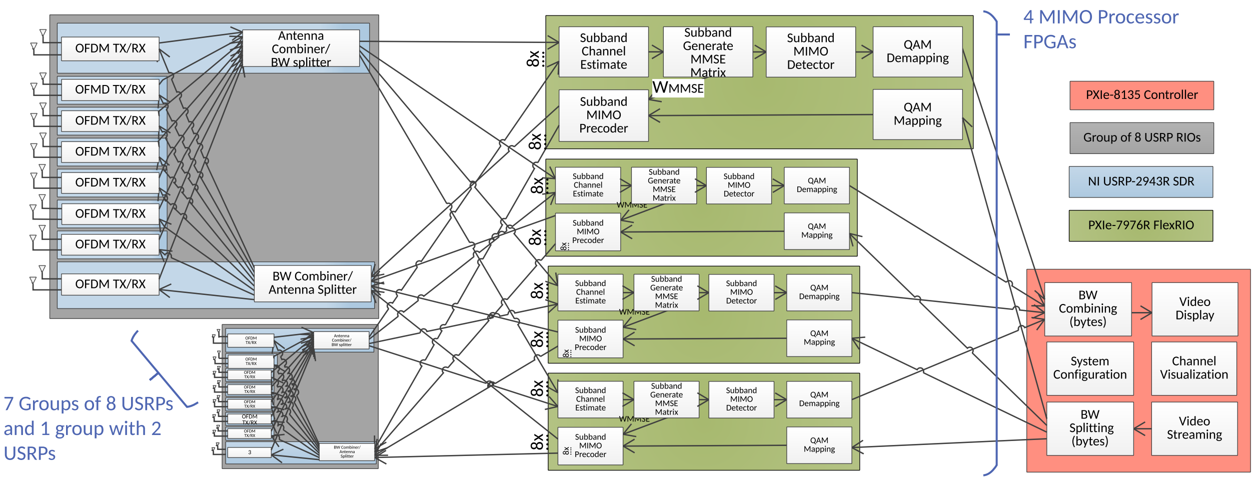

Figure 2.2: Architecture of the LuMaMi BS. The 50 USRPs are divided in groups of 8 to serialize data fed to the MIMO processors implemented on FlexRIOs. Each group splits the overall 20 MHz bandwidth into 4 subbands transferred to the corresponding FlexRIO. On each FlexRIO, the MIMO detection/precoding for all antennas and a quarter of the overall bandwidth is performed. System setup, monitoring and visualization is done from a standard Windows-based host computer.

overall 20 MHz bandwidth. This mitigates implementation constraints of the signal processing (especially processing latency and large-scale matrix arithmetic). Via high-speed routers the data of all the SDR groups is aggregated/disaggregated and detection/precoding as well as symbol mapping/demapping is done.

The host computer configures the system, visualizes system and performance metrics and generates data streams to be transmitted, e.g. HD-video streams or pseudo-random sequences.

2.2 Physical layer specifications

The physical layer protocol adopted for the proof-of-concept experiments described later in Chapter 3, operates with many parameters similar to LTE 20 MHz standard cellular systems. The motivation for this is two fold: *i)* it provides a certain degree-of-confidence to the operation of the system, as it is based on a successful deployed system; *ii)* it showcases that a MaMi processing layer could, in fact, be an add-on feature to existent cellular standards.

2.2.1 Modulation scheme

Orthogonal Frequency Division Multiplexing (OFDM) is used as the modulation scheme in both link directions, i.e. UL and DL. Each resulting sub-channel is processed independently by MaMi TDD-like processing schemes. Table 2.1 summarizes the LTE-like parameters adopted for the OFDM signaling setup.

Table 2.1: OFDM parameters

Parameter	**Variable**	**Value**
Bandwidth	W	20 MHz
Sampling Rate	F_s	30.72 MS/s
FFT Size	N_{FFT}	2048
# Used Subcarriers	N_{used}	1200
1-Side Guard Subcarriers	N_{Guard}	424
Carrier Frequency	f_c	3.7 GHz

2.2.2 Frame structure

Given the modulation scheme, the frame structure is as follows. The transmission is divided into 10 ms radio frames as shown in Fig. 2.3. The frame consists of 10 subframes, each containing two 0.5 ms slots. The radio frame starts with a special DL broadcasting subframe, which in fact consists of PN sequences, to setup the initial synchronization of the network. In our case, they are used to mitigate frequency offsets between the BS and the UEs, and to provide UEs with a reference signal for the timing of the frame structure.

The remaining 9 subframes are used for UL and DL data transmission. As also demonstrated in Fig. 2.3, one slot consist of 7 OFDM symbols, where the 1st is used entirely for UL pilots, followed by 2 UL data symbols, a guard period for UL DL switching, and 2 DL data symbols, followed by a guard period for DL UL switching. For completeness, Table 2.2 summarizes the parameters of the frame structure used. We remark that, a slot dedicated for reciprocity calibration is not included in our frame structure sketch. The main reason is that, from our experience with the testbed, calibration only needs to be performed on an hourly basis given a stable system temperature. Thus, in our experiments we calibrate once after boot up and use the obtained calibration weights throughout a whole measurement[1]. Different boot ups can thus occur in between measurement sessions.

A remark about the maximum users mobility that can be supported with the current physical layer specifications follows. Assuming that channel aging is the main impairment that constrains mobility, the maximum mobility supported is mainly determined by the pilot rate and carrier

[1]Information about the measurements is given in Chapter 3.

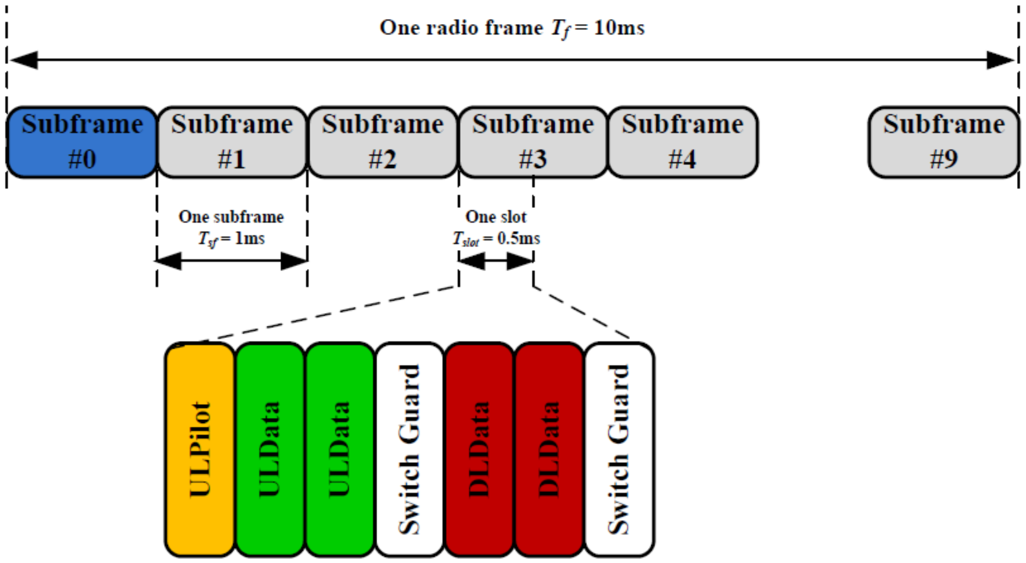

Figure 2.3: Frame structure.

frequency. In our case, we transmit uplink pilots symbol every 0.5 ms and have a wavelength of about 8 cm. If it is assumed that the channel is outdated half-a-wavelength away from the original channel estimation position, then speeds to up 288 km/h can be supported. This rule-of-thumbs provides a rough indication that both pedestrian and vehicular mobility can, in fact, be supported although we note that other factors as the channel richness and number of BS antennas also influence the maximum supported speeds.

Table 2.2: Frame structure parameters

Parameter	**Variable**	**Value**
Slot time	T_S	0.5 ms
Sub-frame time	T_{sf}	1 ms
Frame time	T_f	10 ms

2.2.3 Channel estimation and payload data transmission

The OFDM UL channel estimation time/frequency grid adopted is as follows. Each user has a number subcarriers reserved for uplink channel estimation, which are uniformly spaced across the bandwidth. More specifically, the spacing between available subcarriers for a given user is KF_s/N_{FFT}. As a result, all K users perform channel estimation at the same time, but are only interleaved in frequency. The BS performs least-squares based channel estimation, and interpolates the estimates between pilot symbols using zero-order hold. Reciprocity calibration is then performed independently per subcarrier. This calibrated version of the DL channel is then used to construct a proper precoding matrix.

Pilot symbols are precoded in the DL in the same time/frequency slot for all users. Each user estimates is respective DL channel by simply dividing the received pilots with the *true* pilot value at each sub-carrier. Downlink pilot symbols are precoded in the DL and each user performs least-squares based channel estimation. Using the estimates, each user recovers the payload data using a one-tap equalizer.

2.2.4 MIMO aspects

Let $\mathbf{H}$ denote the $M \times K$ estimated uplink channel matrix, and $\beta_{\mathbf{reg_{pre}}}$ and $\beta_{\mathbf{reg_{dec}}}$ be positive regularization scalar constants. For DL transmission, we pre-multiply $\mathbf{H}$ with a diagonal $M \times M$ calibration matrix $\mathbf{C}$ to compensate for the non-reciprocity of the channel [1]. Let this product be denoted by $\mathbf{H_c} = \mathbf{CH}$. Table 2.3 summarizes the three different linear precoder and detection schemes used in our experiments. We remark that only MR and ZF were considered in the experiments reported next. Nevertheless, RZF is also a feature of the testbed. All our experiments used $M = 100$ BS antennas and up to $K = 12$ simultaneous users.

Table 2.3: Linear Precoding/Detection Schemes

	MR	**ZF**	**RZF**
DL Precoder	$\mathbf{H_c^*}$	$\mathbf{H_c^*}(\mathbf{H_c^T}\mathbf{H_c^*})^{-1}$	$\mathbf{H_c^*}(\mathbf{H_c^T}\mathbf{H_c^*} + \beta_{\mathbf{reg_{pre}}}\mathbf{I}_K)^{-1}$
UL Detector	$\mathbf{H}^H$	$(\mathbf{H}^H\mathbf{H})^{-1}\mathbf{H}^H$	$(\mathbf{H}^H\mathbf{H} + \beta_{\mathbf{reg_{dec}}}\mathbf{I}_K)^{-1}\mathbf{H}^H$

Chapter 3

Testbed experiments

There are many different experiments that can be done with a testbed to demonstrate the operation, assess the performance, and identify potential problems of MaMi in real propagation environments. Some of the debated properties of MaMi deals with what gains can be achieved in real propagation environments and especially in highly mobile scenarios.

Here we show a number of characteristic experiments performed as a part of the testbed based proof-of-concept studies in MAMMOET. The tests include spatial multiplexing of many terminals, both in indoor and outdoor scenarios. During the indoor scenario tests, performed in cooperation with University of Bristol, two separate spectral efficiency world records were obtained. The second one almost doubling the first one, from 79 bit/sec/Hz to 145 bit/sec/Hz. The mostly stationary outdoor tests were done as a preparation for the more thorough mobility tests. The last set of tests, showing that MaMi can handle high mobility, were also performed in cooperation with University of Bristol. The mobility of users is increased from slow/pedestrian all the way up to speed of around 50 km/h. [1]

3.1 Spatial multiplexing of static terminals

3.1.1 Indoor

The indoor tests were performed in a lecture hall at Lund University. The two main objects were to show, that (i) MaMi is capable of serving 12 single-antenna UEs at the same time and frequency resources (ii) evaluate performance differences between spatial MR and ZF in realistic propagation environment. Figure 3.1a shows the setup of the measurement. The 12 UEs were placed in groups of four with a high density of UEs in each group as shown in Figure 3.1b. Two independent tests were performed. First, all UEs were set up and their TX gains were swept over a range from 0 to 30 dB to evaluate the UL performance. Second, the UEs were set to a good TX gain to achieve a high-quality UL channel estimate and then the BS TX gain was swept from 0 to 30 dB to evaluate the DL performance. In the test, all UEs transmit at the same output power and no UL power control scheme has been adopted.

Looking at the UL BERs for QPSK and 64-QAM modulation while utilizing ZF detection in Figure 3.2, it is visible that separation of UEs is possible with some spread in the performance over the different UEs. For the UEs in the group furthest away, i.e. UE0 and UE1 a sudden increase to a BER of 0.5 is noticeable which is due to a saturation in the TX of these UEs.

[1] The physical restraints of the closed-off parking lot where the tests were performed prevented us from reaching speeds higher than 50 km/h.

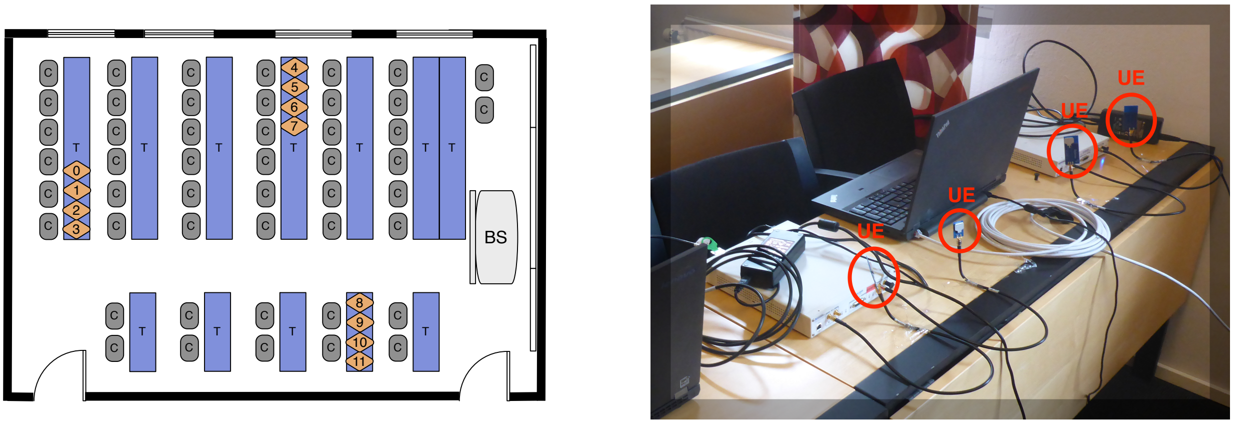

(a) (b)

Figure 3.1: (a) The lecture room where the indoor measurements were performed including the positions of the 12 UEs. (b) One group of four closely spaced UEs.

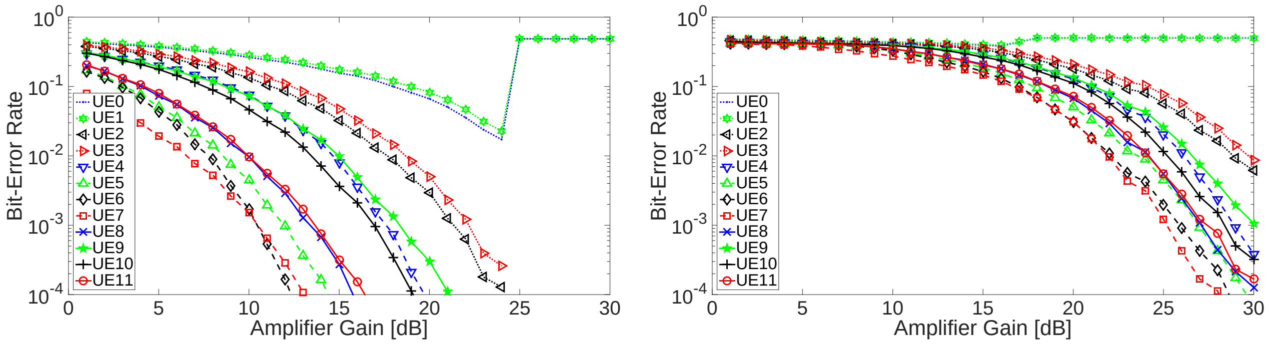

(a) (b)

Figure 3.2: UL BERs for 12 UEs and ZF decoder. (a) using QPSK and (b) using 64-QAM.

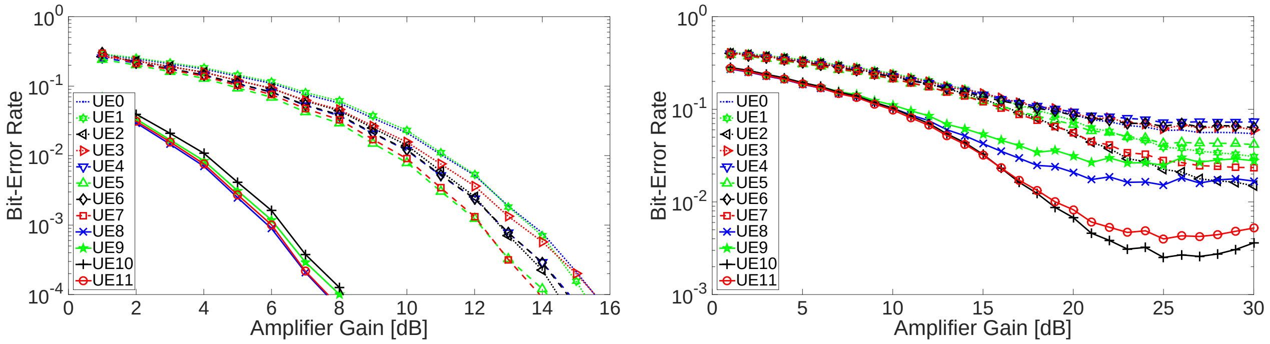

(a) (b)

Figure 3.3: DL BERs for 12 UEs and ZF decoder. (a) using QPSK and (b) using 64-QAM modulation.

The DL BERs for QPSK and 64-QAM and ZF precoding are shown in Figure 3.3. Here, a large gap in performance is visible between the four closest UEs and the other further away. In the 64-QAM case, the overall performance is deteriorated with the BERs flooring at higher gain values. Comparing to the UL, more errors are experienced in the DL and the error-floor is likely a result of imperfect reciprocity calibration during this measurement.

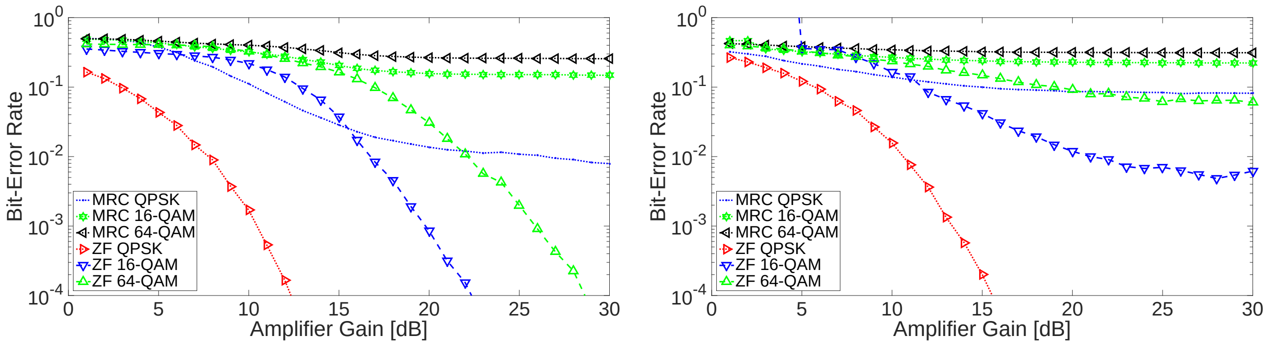

(a) (b)

Figure 3.4: BERs for UE 11 using QPSK, 16-QAM and 64-QAM modulation. (a) on the UL for ZF and MRC detector and (b) on the DL for ZF and MRT precoder.

Comparing the performance between MRC and ZF for UE4, as shown in Figure 3.4 it is clearly visible that there are significant differences in performance. The BERs for MRC on the UL and DL floor at higher gain values while ZF is achieving really low BERs on the UL. On the DL, even ZF shows significant performance loss for 16-QAM and 64-QAM, again introduced by interference due to inaccuracies in the reciprocity calibration.

In an other indoor measurements test outside MAMMOET, performed in collaboration with University of Bristol in Bristol, their MaMi testbed using the same code base but with 128 antennas was used to find the maximum number of UEs separable (in that particular system setup and propagation environment) in an UL only scenario.

Figure 3.5a shows the University of Bristol MaMi testbed with its 128 antenna element patch antenna array. The 22 static UEs were packed very closely resulting in a very high UE density shown in Figure 3.5b. A picture of the overall setup in Figure 3.5c details the setup from a BS perspective were the BS antenna array and the UEs positioned abut 20 meters away are visible. The resulting 22 256-QAM constellation transmitted to the BS on the UL are depicted in Figure 3.5d. It is needed to be pointed out that this is an uncoded transmission an clear received constellations are observed. Considering the transmission from all 22 UEs, a spectral efficiency of 145 bit/s/Hz is achieved which is about 22 times the spectral efficiency of single-stream LTE systems and a new world record. The uncoded BER and the overhead for UL pilot transmission have been taken into consideration in the spectral efficiency calculation.

3.1.2 Outdoor

In this setup, the BS was placed on the rooftop of the department building (Department of Electrical and Information Technology, Lund University) while the UEs were situated on the opposite wing in a distance of about 15 to 20 meters to the BS, as shown in Figure 3.6. In this test, QPSK modulation and uncoded transmission were adopted.

Figure 3.7 shows two pictures taken from this scenario, one from the BS side and one from the view of one of the UEs. In both locations, the visible UEs and the BS were marked.

In this scenario, separating 6 UEs at the same time and frequency source and without error-correction coding was not possible using MRC, due to the significant inter-UE interference (see Figure 3.8a). However, when employing ZF detection, up to 8 UEs were clearly separable showing good constellation diagrams (see Figure 3.8b).

Similarly, DL transmission with MRT experienced strong inter-UE interference and no clear constellation diagram can be observed at the UE. On the other hand, ZF showed a relatively

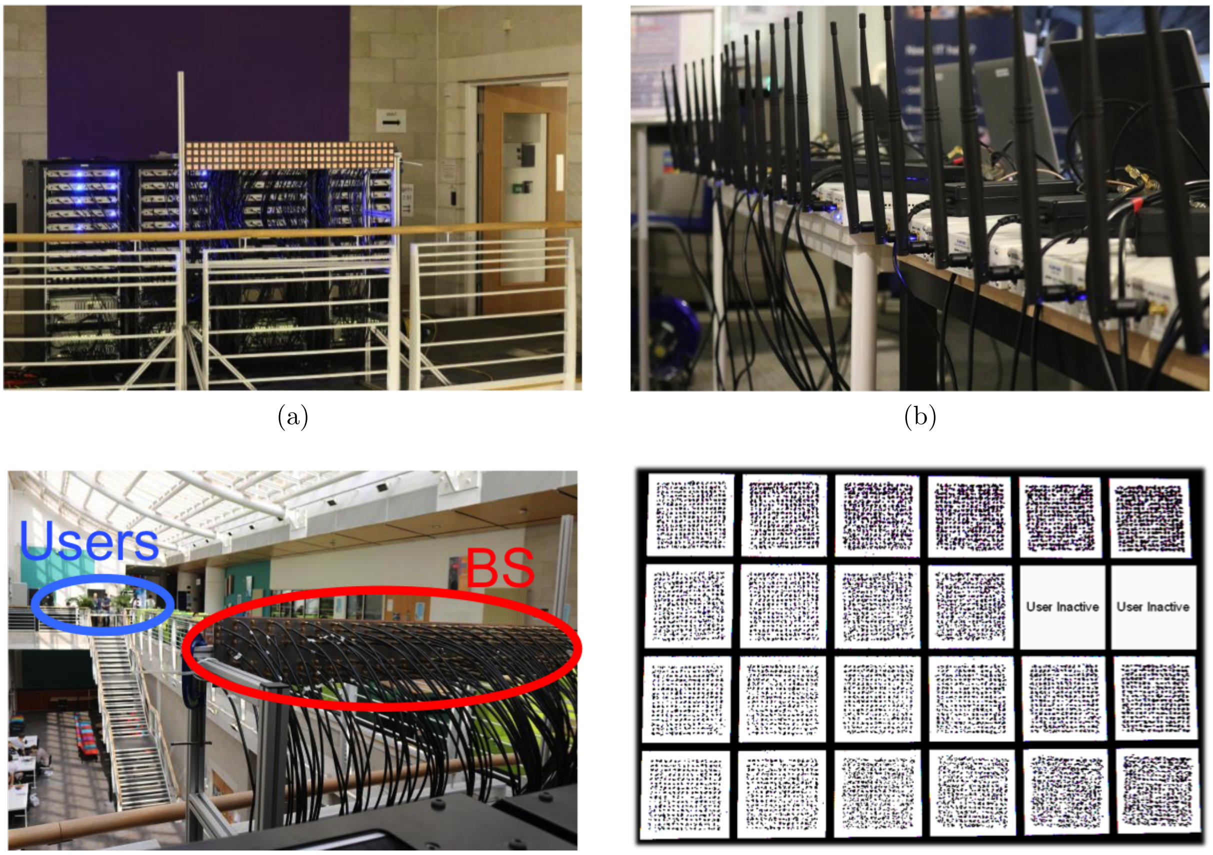

(a) (b) (c) (d)

Figure 3.5: The setup for the measurements performed at University of Bristol: (a) The Bristol MaMi testbed with 128 antennas, (b) the 22 closely spaced UEs, (c) the full setup from the BS view with the UEs positioned about 20 meters away and (d) the 22 256-QAM constellations transmitted on the UL.

good performance on the DL, as shown in Figure 3.9.

3.2 Spatial multiplexing in mobile environments

3.2.1 Measurement setup

Here we describe the measurement environment chosen, and the BS and terminal setup used to provide a certain degree-of-mobility to UEs. We end with a short description of several measurement scenarios.

Measurement environment

The measurements were carried out in the parking lot the E-building of the Faculty of Engineering of Lund University. More specifically, the BS is placed at one of the rooftops of the E-building with the antenna array facing the parking lot area where UEs are distributed. The parking lot was closed off for the tests and UEs were distributed in the range of 30–70 m from the BS. Fig. 3.10 shows photographs of the BS placement on the roof and of the parking lot where the UEs were placed/moving around, as seen from the BS.

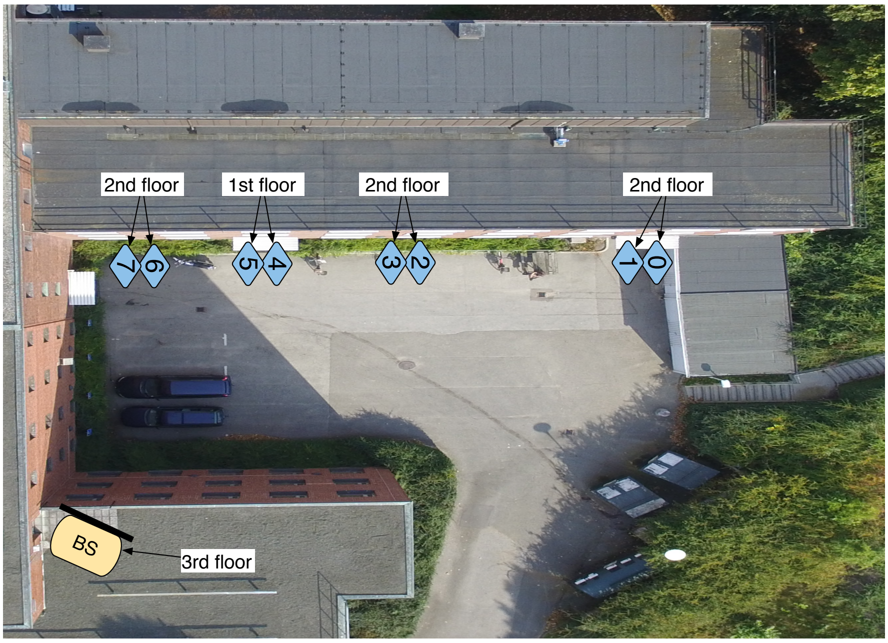

Figure 3.6: Scenario for the outdoor tests. BS placed on the rooftop of the building (third floor) serving eight UE on the opposite wing, with six UE on second floor and two UEs on first floor.

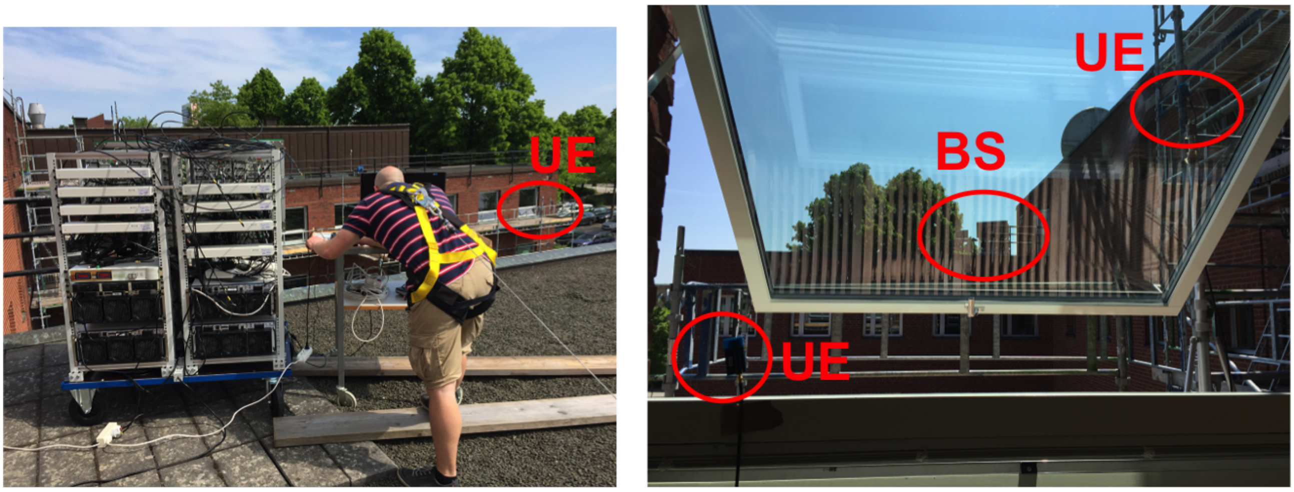

(a) (b)

Figure 3.7: The outdoor test scenario setup: (a) the BS deployed on the rooftop of the department building marked with two UEs on the opposite building wing and (b) view from the perspective of two marked UEs also including the BS on the opposite building wing.

System aspects

The BS (and UEs) computes channel estimates and uncoded BER curves in real time. These are logged every 5 ms, with one entire measurement session lasting one minute. The transmit power of each USRP is about 5 dBm.

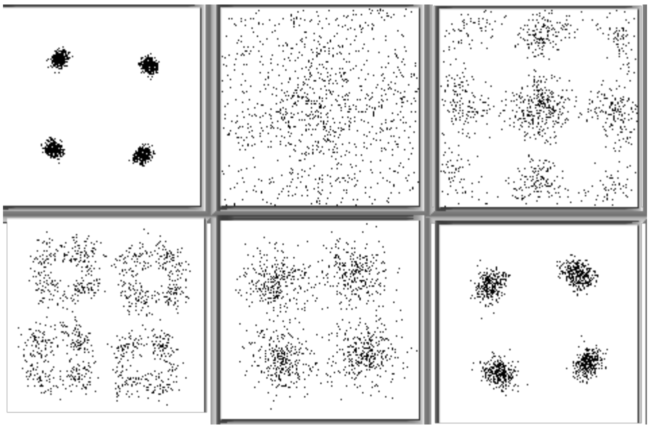

(a)

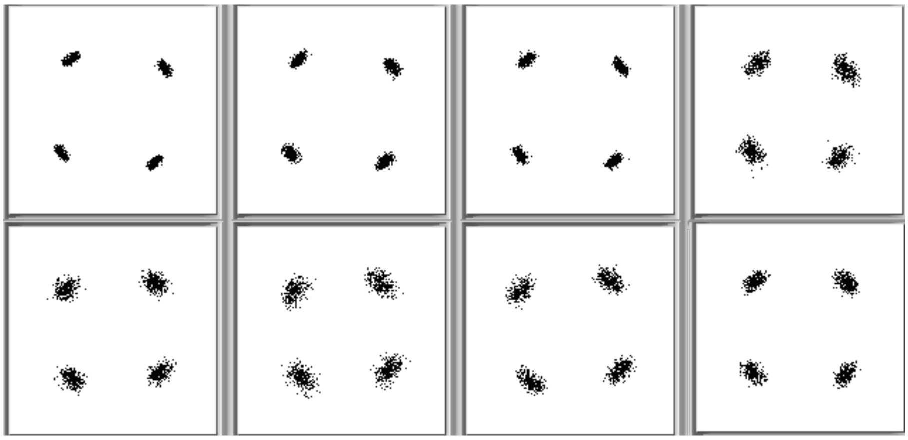

(b)

Figure 3.8: UL constellations (2400 per diagram) for the outdoor experiment (QPSK modulation used): (a) when using MRC with 6 UEs and (b) when using ZF to serve 8 UEs.

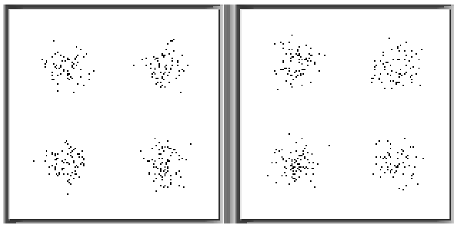

(a)

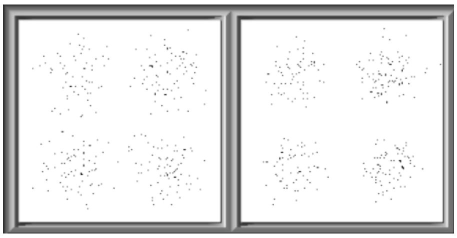

(b)

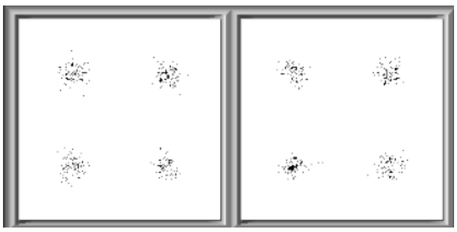

(c)

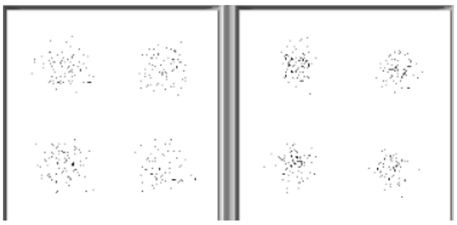

(d)

Figure 3.9: Received DL constellations (2400 per diagram) using ZF: (a) UE0 & UE1 (b) UE2 & UE3 (c) UE5 & UE8 and (d) UE9 & UE10.

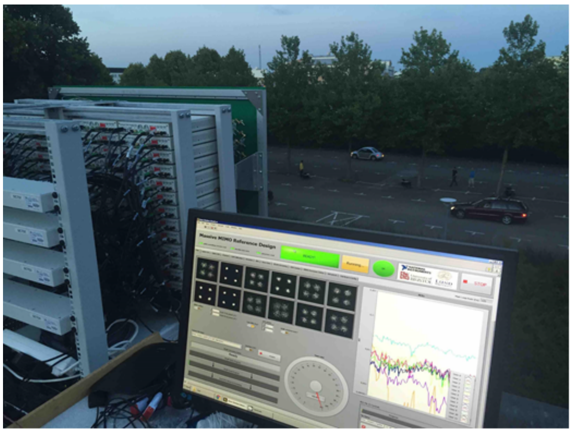

Figure 3.10: Left: BS placed on a rooftop. Right: View from the BS to the parking lot where users are distributed.

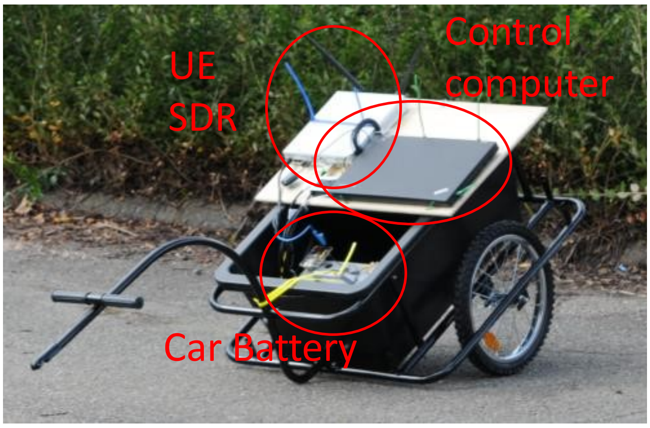

Figure 3.11: Bicycle cart setup for a UE in a bicycle cart.

BS array setup

The dimensional layout of the array adopted for this work corresponds to the 4×25 rectangular grid in the upper part of the array shown in Fig. 2.1. Only one antenna port is used per antenna element, and the unused ports are terminated with matching loads. For a given antenna, the polarization port is chosen such that its adjacent antennas – the antennas spaced by half wavelength, which are four at most – are cross-polarized. This setting provides, so-called, polarization diversity. This is crucial since the orientation of user terminals is typically random. More information about the antenna array can be found in [2].

UE setup

Each of the K UEs uses a linearly polarized near omni-directional antenna. One USRP has two RF chains and thus it can emulate at most two UEs. To enable mobility, two types of UEs are set up: *i)* the first type of UE is mounted on bicycle carts, as shown in Figure 3.11. Each bicycle cart has two single-antenna UEs powered by car battery. This type of UE was moving at pedestrian speed during the tests; *ii)* the second type of UE is placed in cars, as shown in Figure 3.12, where the antennas were mounted at the car top and the USRP was placed at the back trunk.

(a) (b)

Figure 3.12: The UE setup on a car: (a) shows the antennas for two single-antenna UE on the car and (b) shows the corresponding USRP and battery for the UEs.

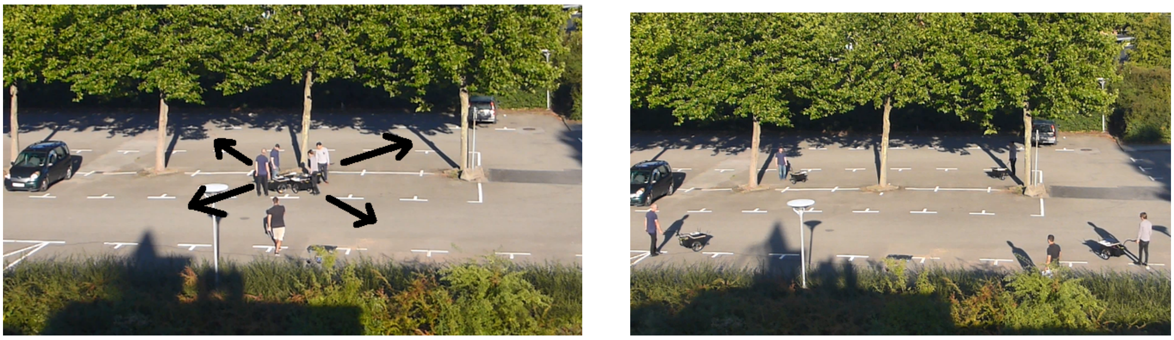

(a) (b)

Figure 3.13: Low mobility measurement: (a) User distribution at the beginning of the measurement and (b) User distribution at the end of the measurement.

3.2.2 Scenario I: Low mobility - Pedestrian speed UEs

One scenario considered was moving users at pedestrian-like speeds. One example of such measurement is depicted in Figure 3.13. The measurement starts with users closely positioned, which move slowly in the opposite directions to the center. Since channel measurements are collected as users are being spread away, the goal of the measurements is to obtain insights to what kind of user density can be supported in a practical system.

3.2.3 Scenario II: High mobility - Vehicular and pedestrian speeds UEs

The second scenario focused in high mobility environments, where several users operate at speeds of around 50 km/h. One such test experiment is depicted in Figure 3.14, where it shows the mobility pattern of 12 UEs in this measurement. Eight UEs are placed on four bicycle carts and moving randomly in the middle of the parking lot, and 4 UEs are placed in two cars driving around the parking lot. In the test, all 12 UEs can be successfully decoded in such mobile scenario.

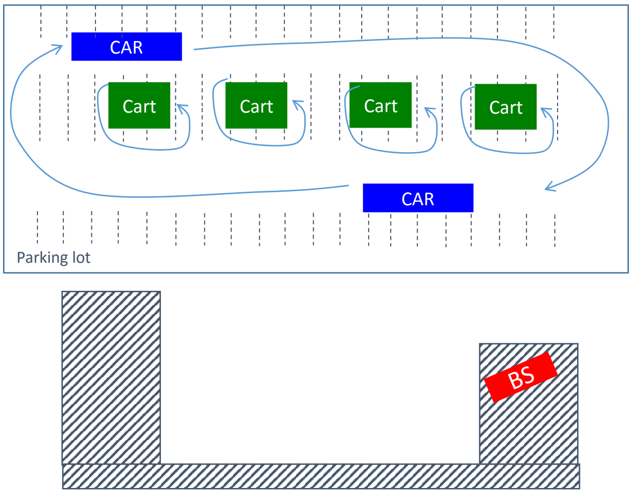

Figure 3.14: Scenario for the outdoor mobility tests (not to scale). A BS placed on the rooftop of the building (third floor) serving 12 UEs on the parking lot, with 8 UEs on bicycle carts and 4 UEs on cars.

3.2.4 Link to proof-of-concept footage

A link to the videos taken during the experiments can be found in [3]. It provides live footage from the whole measurement procedure, including real-time channel metrics and communication error metrics.

Chapter 4

Conclusions

The proof-of-concept studies in MAMMOET includes both the design of a real-time MaMi testbed, operating with 100 antennas in TDD mode using an LTE-like physical layer, and the communication tests performed using the testbed. The design and successful operation of this testbed shows that it is possible to implement a MaMi system, with generic programmable commercial off the shelf (COTS) hardware, capable of reaching extreme performance in terms of spectral efficiency, handling real propagation environments and mobility up to at least 50 km/h.

Since MaMi implemented with dedicated hardware will be much more streamlined and efficient than a testbed based on generic COTS hardware, the proof-of-concept studies also show indirectly that commercial MaMi systems delivering large gains in both spectral and energy efficiencies should be quite feasible.

One of the things that we have not yet tested is the achieved communication range. This has two reasons: i) The tests were performed in a closed-off parking lot (ranges limited to around 70 m) and ii) using only full data-rate to all users (entire 20 MHz band), the available transmit power on the testbed does not allow for any longer ranges. When investigating communication range, tests should be done so that data-rate can be traded for range so that the relationship between the two can be studied. Such tests have not been done yet.

Chapter 5

List of Abbreviations

BER	Bit Error Rate
BS	Base Station
COTS	Commercial Off the Shelf
DL	Down-Link
EC	European Commission
FPGA	Field-Programmable Gate Array
MaMi	Massive MIMO
MIMO	Multiple-Input Multiple-Output
MMSE	Minimum Mean-Squared Error
MR	Maximum-Ratio
MRC	Maximum-Ratio Combining
MRT	Maximum-Ratio Transmission
OC	OctoClocks
OFDM	Orthogonal frequency-division multiplexing
PPS	Pulse-Per-Second
QAM	Quadrature Amplitude Modulation
QPSK	Quadrature Phase Shift Keying
RF	Radio Frequency
RZF	Regularized Zero-Forcing
SDR	Software-Defined Radio
SNR	Signal-to-Noise Ratio
TDD	Time-Domain Duplex
TX	Transmit
UE	User Equipment
UL	Up-link
USRP	Universal Software Radio Peripheral
ZF	Zero Forcing

Bibliography

[1] J. Vieira, F. Rusek, O. Edfors, S. Malkowsky, L. Liu, and F. Tufvesson, "Reciprocity calibration for massive MIMO: Proposal, modeling and validation," 2016.

[2] J. Vieira, S. Malkowsky, K. Nieman, Z. Miers, N. Kundargi, L. Liu, I. Wong, V. Öwall, O. Edfors, and F. Tufvesson, "A flexible 100-antenna testbed for massive MIMO," in *2014 IEEE Globecom Workshops (GC Wkshps)*, pp. 287–293, Dec 2014.

[3] "Massive MIMO mobility tests." https://www.youtube.com/watch?v=wPPMrr4rHmo.